Mechanism and Machine Theory

Analysis of hybrid vehicle transmissions with any number of modes and planetary gearing: kinematics, power flows, mechanical power losses.

--Manuscript Draft--

Manuscript Number:	
Article Type:	Research Paper
Keywords:	power-split CVT; multimode transmission; analysis; planetary gearing; Hybrid Electric Vehicle; Cadillac CT6
Corresponding Author:	Marco Cammalleri University of Palermo Palermo, Palermo ITALY
First Author:	Marco Cammalleri
Order of Authors:	Marco Cammalleri
	Antonella Castellano, PhD student
Abstract:	This paper is focused on upgrading a unified parametric model, available in the literature, that can perform both the analysis and the design of Power-Split Continuously Variable Transmissions (PS-CVTs), which are particularly promising to deploy in the hybrid electric powertrain. In particular, a new procedure for the identification of the basic functional parameters underlying the model is presented. This new method does not rely on a case-specific formulation, thus befits any power-split transmission, regardless of the number of planetary and ordinary gear sets and their constructive arrangement. Moreover, it handles the clutches operations that perform the shift between different constructive layouts, therefore it is suitable even for multimode PS-CVTs. As a case study, we applied it to the complex multimode PS-CVT of the Cadillac CT6 and carried out a comprehensive analysis of its kinematics, mechanical power losses and power flows.
Suggested Reviewers:	Ettore Pennestrì full professor, University of Rome Tor Vergata: Universita degli Studi di Roma Tor Vergata pennestri@mec.uniroma2.it He is a very qualified researcher about mechanical transmission.
Opposed Reviewers:	

Dear editor, prof. Paulo Flores,
I'm pleased to submit our new work about power-split CVTs. Within this paper, we provide a new procedure for the identification of the basic functional parameters underlying the innovative model about the design and analysis of PS-CVTs, which was the subject of three papers already published in your Journal:

[1] Cammalleri M., Rotella D., "Functional design of power-split CVTs: An uncoupled hierarchical optimized model", Mech. Mach. Theory 116 (2017) 294–309.
[2] D. Rotella, M. Cammalleri, Direct analysis of power-split CVTs: A unified method, Mech. Mach. Theory 121 (2018) 116–127.
[3] Rotella D., Cammalleri M., Power losses in power-split CVTs: A fast black-box approximate method, Mechanism and Machine Theory 128 (2018) 528–543, https://doi.org/10.1016/j.mechmachtheory.2018.06.011

Therefore, it would be convenient to submit also this paper to the same reviewers of the previous papers. Hoping both you and reviewers will find also this new manuscript suitable for publication, I look forward to hearing from you.

Best regards
Marco Cammalleri

Highlights

- A unified parametric model for power-split transmissions is upgraded.
- A new method for identifying the basic functional parameters is presented.
- The procedure is easily automatable for any number of planetary gears and modes.
- The model does not require any case-specific formulas.
- An exhaustive analysis of the Cadillac CT6 multimode transmission is performed.

Analysis of hybrid vehicle transmissions with any number of modes and planetary gearing: kinematics, power flows, mechanical power losses.

Marco Cammalleri [1], Antonella Castellano[2]
[1,2] Department of Engineering, University of Palermo, Italy.
Email: [1]marco.cammalleri@unipa.it, [2]antonella.castellano@unipa.it
Corresponding author: Marco Cammalleri. Tel.: +39 091 23897256

ABSTRACT

This paper is focused on upgrading a unified parametric model, available in the literature, that can perform both the analysis and the design of Power-Split Continuously Variable Transmissions (PS-CVTs), which are particularly promising to deploy in the hybrid electric powertrain. In particular, a new procedure for the identification of the basic functional parameters underlying the model is presented. This new method does not rely on a case-specific formulation, thus befits any power-split transmission, regardless of the number of planetary and ordinary gear sets and their constructive arrangement. Moreover, it handles the clutches operations that perform the shift between different constructive layouts, therefore it is suitable even for multimode PS-CVTs.

As a case study, we applied it to the complex multimode PS-CVT of the Cadillac CT6 and carried out a comprehensive analysis of its kinematics, mechanical power losses and power flows.

KEYWORDS: power-split CVT, multimode transmission, analysis, planetary gearing, Hybrid Electric Vehicle, Cadillac CT6.

1. INTRODUCTION

Significant efforts have been made in recent years to reduce emissions coming from the automotive field. To comply with the emission limit values imposed by national and international law, more and more car manufacturers have been expanding their product range by introducing powertrain electrification. In this perspective, Hybrid Electric Vehicles (HEVs) are emerging as the eco-sustainable solution bound to become the most widespread in the very short term [1], [2], [3].

The power-split powertrain is the most promising hybrid technology because it decouples the Internal Combustion Engine (ICE) speed from the wheels one (like in series hybrid) and it enables the ICE to feed both the electric unit and the wheels (like in parallel hybrid), even simultaneously [4]-[8]. The power flows, generated by the propulsors and transmitted to the wheels or the battery pack, are handled by the Power-Split Unit (PSU), consisting of Planetary Gear sets (PGs) and fixed-ratio Ordinary Gear trains (OGs). The electric unit relies on two electric machines, which can act as motors for supporting the ICE in vehicle propulsion or as generators for recharging the batteries. Their combined use at variable speed is equivalent to a Continuously Variable Unit (CVU) since it performs kinematically the same role of a mechanical or hydraulic speed variator in Power-Split Continuously Variable Transmissions (PS-CVTs).

The simpler PSU arrangement includes only one PG and it is known as Shunt PS-CVTs (input-split or output-split) while a more complex mechanical layout with two or more PGs leads to Compound PS-CVTs. Furthermore, the embedding of a clutches system results in multimode transmissions, which can generate several internal power flows that better meet the requirements of different driving operations. This enables the minimization of the power size of the electric unit, at the expense of constructive simplicity [9], [10], [11].

To date, several authors have proposed a wide variety of methods for studying PS-CVTs [12]-[35], even though very few of them are effective at both analyzing and designing any PSU, constructive complexity notwithstanding. Numerous papers are very well detailed (for example [24]-[28]) and able to describe some of the key features of specific case studies, but they are lacking in generality. In this scenario, an interesting unified approach was presented for the first time in [36], based on a few functional parameters having a direct physical meaning. Among the main novelties presented, there was the introduction of a powerful design tool, called design-chart, which allows the designer to visually assess all the eligible constructive solutions for PGs and consciously select the best PS-CVT layout. However, the same functional parameters are important for analysis purposes too, since they enable the direct calculation of speed, torque, and power flow of any shaft of the transmission. Therefore, the same authors in [37] addressed a procedure for identifying these functional parameters starting from the constructive layout of any power-split transmission with one or two PGs. Lastly, [38] expanded the features of the model with a straightforward calculation of the mechanical power losses occurring in the PSU and of the real power flows.

In this paper, we present an alternative and more direct approach to calculate the functional parameters from the constructive ones. Unlike the previous formulation [37], it works regardless of the number of PGs and the operating

modes and it does not require any preliminary analysis about the functional scheme under examination, nor a standardization procedure for the Willis' ratios.

The paper is organized as follows. The fundamental equations underpinning the parametric model [36] are reported in section 2. This section also briefly summarizes the swift method addressed in [38] for the calculation of the PSU power losses. Section 3 shows that, with minor changes, the addressed model is suitable also for analyzing the transmission in full electric operation. Section 4 presents the novel method to calculate the new functional parameters. Lastly, the effectiveness of the new procedure and the functionality of the whole model are tested in section 5 by conducting a comprehensive analysis of the complex three-PG multimode PS-CVT of the Cadillac CT6.

Nomenclature

Acronyms:

CVU	Continuously Variable Unit
FEV	Full Electric Vehicle operation
HEV	Hybrid Electric Vehicle
ICE	Internal Combustion Engine
OG	Ordinary Gear set
PG	Planetary Gear set
PS-CVT	Power-Split Continuously Variable Transmission
PSU	Power-Split Unit
TPM	Three-Port Mechanism

Subscripts:

C, R, S	Carrier, Ring gear and Sun gear of a PG
in, out, i, o, n	main ports of the PSU
x, y, z	branches of a TPM
X, Y, Z	shafts of a PG

Symbols:

Overlined powers or torques refer to real working condition

$[\mathbf{K}]$	matrix of constructive constraints
$\{\boldsymbol{\omega}\}$	vector of rotational speeds
k_x	fixed-ratio gear on the *x*-th branch of a TPM
N_C	number of constructive constraints
N_{TPM}	number of Three-Port Mechanisms
P_j	power flowing through the *j*-th branch
p_j	power flowing through the *j*-th branch as a fraction of the input power
p'_j	power flowing through the *j*-th branch as a fraction of the output power
$P_j\big\vert_i$	power flowing through the *j*-th branch of the *i*-th TPM
$\bar{P}_L$	mechanical power losses
$\bar{p}_L$	mechanical power losses as a fraction of the input power
$\bar{p}'_L$	mechanical power losses as a fraction of the output power
T_j	torque applied to the *j*-th shaft
η	overall apparent efficiency
η_0	basic efficiency of a PG
$\eta_{Y/X}^{Z}$	fixed-*Z* apparent efficiency of a PG
$\eta_{X/x}$	apparent efficiency of the *x*-th OG
Θ	torque applied to the *out* shaft as a fraction of the input torque (overall torque ratio)
θ_j	torque applied to the *j*-th shaft as a fraction of the input torque

τ	overall speed ratio
τ_j	speed ratio of the *j*-th shaft
$\tau_{\#j}$	overall speed ratio for which the *j*-th shaft is motionless (nodal ratio)
$\tau_{j\#k}$	speed ratio of the *j*-th shaft when the *k*-th shaft is motionless (corresponding speed ratio)
τ_*	overall speed ratio for which a PG is synchronous
$\phi^z_{x/y}$	generalized characteristic function of a TPM
Ψ	Willis' ratio of a PG
$\psi^Z_{Y/X}$	fixed-*Z* speed ratio of a PG
ω_j	rotational speed of the *j*-th shaft

2. THEORETICAL BACKGROUND

This section summarizes the essentials of the parametric model for PS-CVTs (Fig. 1) presented in [36] by changing both the independent variables and the functional parameters, to align it with the treatment addressed in [38]. Indeed, [36] used a normalized speed ratio as a variable and CVU speed ratio and ratio spreads as functional parameters, which are well suited for a passive mechanical CVU with one Degree Of Freedom (DOF). On the other hand, [38] did not normalize the speed ratio and introduced new basic parameters that better befits the electric CVU behavior with two DOFs.

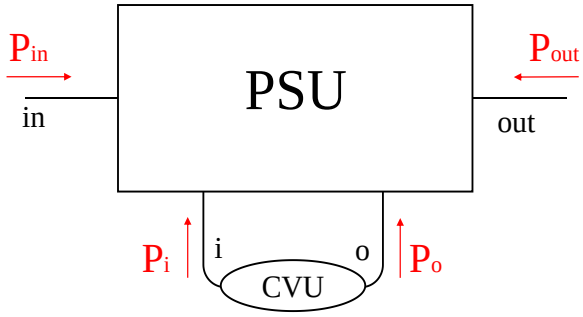

Fig. 1. Schematic layout of a PS-CVT.

Any PSU is a combination of planetary gear sets, whose branches rotate at linearly dependent speeds, ordinary gear sets, whose shafts have proportional speeds, and isokinetic joints, consisting of two or more shafts rotating at the same speed. Consequently, for some PSU shafts their rotational speed is proportional to the input speed (ω_{in}), for others to the output speed (ω_{out}), for still others it is a linear combination of both. In general, the rotational speed of any *j*-th PSU shaft can be normalized to the input speed and written as:

$$\tau_j = \frac{\omega_j}{\omega_{in}} = A_j + B_j\,\tau \tag{1}$$

where τ is the overall speed ratio, defined as the speed ratio between PSU output and input shafts ($\tau = \omega_{out}/\omega_{in}$), and A_j or B_j can be zero. The overall transmission ratio τ achieved when a generic *k*-th shaft is motionless is called nodal ratio:

$$\tau_{\#k} = \left.\frac{\omega_{out}}{\omega_{in}}\right|_{\omega_k=0} \tag{2}$$

On the other hand, the value of the remaining speed ratios τ_j achieved in correspondence of a nodal ratio $\tau_{\#k}$ is called corresponding speed ratio ($j \neq k$):

$$\tau_{j\#k} = \left.\frac{\omega_j}{\omega_{in}}\right|_{\omega_k=0} \tag{3}$$

2.1 CVU kinetostatics

The nodal ratios referred to the *i* and *o* shafts, connected to the CVU (i.e. the electric unit in HEVs), are also called mechanical points. Mechanical points and CVU corresponding speed ratios are sufficient to comprehensively address the ideal kinetostatics of the electric unit, whichever the PSU layout is. The following equations can be easily derived from Fig. 2:

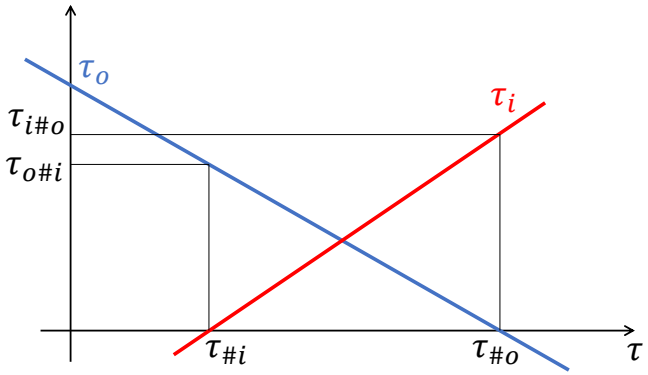

Fig. 2. Example of CVU speed ratios and meaning of mechanical points and CVU corresponding speed ratios.

$$\tau_o = \frac{\omega_o}{\omega_{in}} = \tau_{o\#i}\frac{\tau - \tau_{\#o}}{\tau_{\#i} - \tau_{\#o}} \qquad \tau_i = \frac{\omega_i}{\omega_{in}} = \tau_{i\#o}\frac{\tau - \tau_{\#i}}{\tau_{\#o} - \tau_{\#i}} \tag{4}$$

On the other hand, assuming the conventional sign of the power flowing through the PSU main shafts showed in Fig. 1 the ideal power balance of the PSU can be written as a function of the speed and torque ratios:

$$1 + \Theta\,\tau + \theta_o\,\tau_o + \theta_i\,\tau_i = 0 \tag{5}$$

where:

$$\Theta = \frac{T_{out}}{T_{in}} \qquad \theta_o = \frac{T_o}{T_{in}} \qquad \theta_i = \frac{T_i}{T_{in}} \tag{6}$$

Since the PGs and OGs torques are speed-independent, we obtain the ideal normalized CVU torques θ_o and θ_i as functions of the basic functional parameters by rewriting Eq. (5) in correspondence of the mechanical points.

$$\theta_o = -\frac{1 + \Theta\,\tau_{\#i}}{\tau_{o\#i}} \qquad \theta_i = -\frac{1 + \Theta\,\tau_{\#o}}{\tau_{i\#o}} \tag{7}$$

The power that ideally flows in the CVU shafts can be quickly calculated as a fraction of the input power from the combination of Eqs. (4) and (7):

$$p_o = \tau_o \cdot \theta_o = \frac{(\tau - \tau_{\#o})(1 + \Theta\,\tau_{\#i})}{\tau_{\#o} - \tau_{\#i}} \qquad p_i = \tau_i \cdot \theta_i = \frac{(\tau - \tau_{\#i})(1 + \Theta\,\tau_{\#o})}{\tau_{\#i} - \tau_{\#o}} \tag{8}$$

By introducing the so-called overall apparent efficiency η [38], expressed as the opposite of the output power normalized to the input one, Eqs. (8) can be expressed as functions of η:

$$\eta = -p_{out} = -\frac{P_{out}}{P_{in}} = -\frac{\omega_{out}}{\omega_{in}} \cdot \frac{T_{out}}{T_{in}} = -\tau\,\Theta \tag{9}$$

$$p_o = \frac{(\tau - \tau_{\#o})(\tau - \eta\,\tau_{\#i})}{\tau(\tau_{\#o} - \tau_{\#i})} \qquad p_i = \frac{(\tau - \tau_{\#i})(\tau - \eta\,\tau_{\#o})}{\tau(\tau_{\#i} - \tau_{\#o)}} \tag{10}$$

η is apparent because is not due to power losses but to the active CVU that can assist the ICE or charge the battery. Indeed, an equation similar to Eqs. (10) was obtained also in [20] for a merely mechanical PS-CVT with ideal PSU but passive CVU, by the principle of virtual work, and using ratio spreads as functional parameters.

Eqs. (8) and (10) show that power flows of the electric unit are fully defined by the mechanical points. Thus, selecting mechanical points means establishing the power flowing into the electric machines as a function of the overall transmission ratio τ and the normalized output power (i.e. η) or, alternatively, as function of τ and the overall torque ratio Θ. Once fixed the mechanical points, the definition of the CVU corresponding speed ratios rules the CVU torque ratios. This enables the designer to prioritize the characterization of the electric motors during the design and only then to select the constructive PSU layout since each constructive layout is characterized by univocal functional parameters, but different constructive layouts can be arranged by the same functional parameters.

2.2 PSU characterization

Nodal ratios allow both analyzing and designing any PSU.

Any PSU can be modeled as a combination of Three-Port Mechanisms (TPMs). A generic TPM, enclosed in the dashed-line rectangle of Fig. 3, consists of one planetary gear set (represented by a rounded-corner square) and up to three fixed-ratio gears (rhombi). The constructive parameter that defines a planetary gear train is the Willis' ratio Ψ, while the ordinary gear sets are characterized by the related speed ratio *k*. The power is assumed positive if entering the TPM. Furthermore, Fig. 3 clarifies the nomenclature used for TPMs: the shafts directly linked with the PG are generically indicated by *X*, *Y* and *Z* in capital letters; the shafts connected to the outside of the TPM are indicated by *x*, *y*, and *z* in lowercase letters. In other words, using *X*, *Y* and *Z* is a general way to refer to the PG Ring gear (*R*), Sun gear (*S*) or Carrier (*C*), while *x*, *y* and *z* are related to the PSU main ports (*in*, *out*, *o*, *i*, …) linked to the TPM.

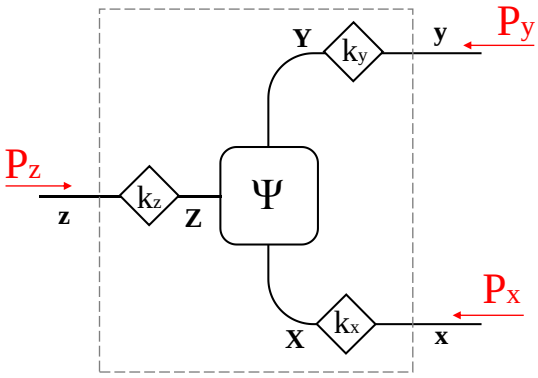

Fig. 3. Generic layout of a Three-Port Mechanism. A rounded-corner square indicates the planetary gear set, rhombi indicate the ordinary gear sets. The external TPM branches are labeled with lowercase letters, the internal TPM branches are labelled with capital letters.

The number of TPMs (N_{TPM}) involved in the PSU equals the number of the shafts whose rotational speed is proportional neither to ω_{in} nor to ω_{out}, but which is a linear combination of both. In other words, each two-way PG whose shafts rotate at non-proportional speeds ensures the existence of a proper nodal ratio (i.e. a finite and non-zero nodal ratio), which can be freely selected during the design. Conversely, the nodal ratios referred to the shafts rotating at speeds proportional to ω_{in} or ω_{out} equal infinity or zero, respectively. Since the PSU has only four externally accessible ports (Fig. 1), a shunt PS-CVT having one TPM has only one proper nodal ratio. Indeed, in input-split CVTs one mechanical point is zero, because a fixed-ratio connection is realized between the output shaft and one of the CVU shafts. On the contrary, in output-split transmissions, where the input shaft is directly connected to *o* or *i* shaft, one mechanical point tends to infinity.

Moreover, the two mechanical points define the CVU power flows, as addressed in section 2.1. Therefore, any further TPM over two affects neither the CVU ideal power flows nor kinematics. Nonetheless, it can be useful to use more than two TPMs to arrange multimode transmission (as in the PS-CVT analyzed in section 5). Using three or more TPMs implies the presence of further main ports, called neutral nodes (*n*), which are isokinetic joints into which two or more branches linked neither with the CVU nor with the input/output of the driveline are merged. The number of the neutral nodes equals the number of each additional TPM over two.

Nodal ratios also govern a set of characteristic functions, defined as the speed ratio between two generic TPM branches when the third one is motionless, to the same speed ratio when the third shaft is moving:

$$\phi^{z}_{x/y} = \frac{\tau_x/\tau_y\big|_{\tau_{z=0}}}{\tau_x/\tau_y} = \frac{\tau_{\#z} - \tau_{\#x}}{\tau_{\#z} - \tau_{\#y}} \cdot \frac{\tau - \tau_{\#y}}{\tau - \tau_{\#x}} \tag{11}$$

Characteristic functions are a crucial tool for this model because they play an important role in both the design and analysis stage.

2.2.1 Characteristic functions and PSU functional design

To minimize the meshing losses of a PG, it should operate as close as possible to its synchronous point within the desired range of operation. For this purpose, the characteristic functions permit the designer to assure this condition, by relating the desired overall transmission ratio for which the PG of a TPM works synchronous (τ_*) with the PG constructive arrangement. Indeed, it is:

$$\phi^{z}_{x/y}(\tau_*) = \frac{\tau_x/\tau_y\big|_{\tau_{z=0}}}{\tau_x/\tau_y\big|_{\tau_*}} = \psi^{Z}_{X/Y} \tag{12}$$

where $\psi^{Z}_{X/Y}$ is the ratio between ω_X and ω_Y of the PG achieved when $\omega_Z = 0$. Since $\psi^{C}_{R/S}$ equals the Willis' ratio Ψ by definition, then, once selected the nodal ratios, the characteristic functions match the synchronous condition τ_* of a PG to its respective Willis' ratio and a feasible connection between its shafts Carrier, Ring, Sun, and the PSU ports (*in*, *out*, *i*, *o*, n_1, …), without directly involving the OGs.

In a preliminary design stage, the property (12) enables the exploitation of the design-chart [36], which allows a quick comparison between the main features of different feasible solutions. The design-chart is a graphical representation of all the PSU characteristic functions that take on values comprised within the desired range of Willis' ratio (preferably from

$-2/3$ to $-1/3$ [38]). Choosing one, two, or N curves of the design-chart means to determinate a feasible layout with one, two, or N TPMs (and thus N proper nodal ratios). Selecting a point from a specific curve means to determine both the PG Willis' ratio and the position of the carrier (linked to the main port *z*), the ring gear (linked to *x*) and the sun gear (linked to *y*), as well as the synchronous point τ_* of a PG.

Generally speaking, the number of characteristic functions grows factorially with the number of TPMs (and therefore of neutral nodes). Indeed, each TPM can be linked to three main ports out of the available (N_{TPM}+2). Furthermore, for each triad of main ports attached to the TPM, there are ${}_3\boldsymbol{P}_3$=6 possible ways to arrange the position of carrier, ring and sun gear. The number of all characteristic functions as a function of N_{TPM} is:

$$\binom{N_{TPM}+2}{3} \cdot {}_3P_3 = N_{TPM} \cdot (N_{TPM}+1) \cdot (N_{TPM}+2) \tag{13}$$

[36] listed explicitly all the 24 characteristic functions for the design of PS-CVTs with up to two active planetary gear trains. However, [38] suggested the more general Eq. (12), which makes the computational process independent from the PSU layout and automatable by a simple permutation of the nodal ratios.

Finally, the ordinary gear sets have the role of tuning the speeds inside the PSU, once chosen the functional parameters and synthesized the PGs [36]. Indeed, imposing a certain synchronous point for the involved PGs results in constraining the fixed-ratio gears of the respective TPM:

$$\frac{k_x}{k_y} = \left.\frac{\tau_x}{\tau_y}\right|_{\tau_*} = -\frac{\tau_{x_{\#y}}}{\tau_{y_{\#x}}} \cdot \frac{\tau_* - \tau_{\#x}}{\tau_* - \tau_{\#y}} \qquad \frac{k_x}{k_z} = \left.\frac{\tau_x}{\tau_z}\right|_{\tau_*} = -\frac{\tau_{x_{\#z}}}{\tau_{z_{\#x}}} \cdot \frac{\tau_* - \tau_{\#x}}{\tau_* - \tau_{\#z}} \tag{14}$$

Using two equations like (14) for each TPM is sufficient to completely arrange the ordinary gear sets.

2.2.2 Characteristic functions and PSU analysis

In an analysis stage, the Willis' ratios of the involved PGs are known parameters as well as the connections between their shafts and the PSU ports. Thus, Eq (11) and Eq. (12) can be used to compute the overall transmission ratio corresponding to the PG synchronism as follows:

$$\tau_* = \frac{\Psi\left(\frac{\tau_{\#z} - \tau_{\#y}}{\tau_{\#z} - \tau_{\#x}}\right)\tau_{\#x} - \tau_{\#y}}{\Psi\left(\frac{\tau_{\#z} - \tau_{\#y}}{\tau_{\#z} - \tau_{\#x}}\right) - 1} \tag{15}$$

where $\tau_{\#x}$ is the nodal ratio referred to the main port linked with the ring gear, $\tau_{\#y}$ is referred to the main port linked with the sun gear and $\tau_{\#z}$ is referred to the main port linked with the carrier.

Furthermore, characteristic functions represent the opposite of the ratios between the ideal powers transmitted by two shafts of a TPM:

$$\phi^z_{x/y} = -\frac{P_y}{P_x} = -\frac{p_y}{p_x} \tag{16}$$

The property (16) is a powerful tool for assessing the ideal power flow distribution in the PSU, as it is addressed in the next section 2.3.

2.3 PSU mechanical power losses

The total power losses of the PSU are the sum of the mechanical losses occurring in every PG and OG. These can be calculated by the swift approximate method proposed in [38], which is ruled by nodal ratios and characteristic functions.

In the following, power losses are normalized to the input power and the power flows and torques referred to the real conditions are indicated by an overline. For an OG linking the branch *x* of the TPM to the shaft *X* of the PG is:

$$\bar{p}_L|_{OG} \approx -\left|\left(1 - \eta_{X/x}\right) p_x\right| \tag{17}$$

where $\eta_{X/x}$ is the OG efficiency, while for a PG it is:

$$\bar{p}_L|_{PG} \approx -\left|\left(1 - \eta^Z_{Y/X}\right)\left(\frac{\phi^z_{x/y} - \psi^Z_{X/Y}}{1 - \psi^Z_{X/Y}}\right) p_x\right| \tag{18}$$

in which p_x is the ideal normalized power flowing through the *x* shaft external to the TPM. When possible, it is more convenient to use for p_x one of the four PSU external shafts because their power flows are known (1 or η) or directly computable (Eqs. (8)-(10)). Otherwise, p_x can be easily calculated by using one equation of power conservation in an isokinetic joint combined with the property (16) of characteristic functions. Moreover, $\psi^Z_{X/Y} = \left(\psi^Z_{Y/X}\right)^{-1}$ is the fixed-*Z* speed ratio of the PG and $\eta^Z_{Y/X} = \left(\eta^Z_{X/Y}\right)^{-1}$ its related apparent efficiency, i.e.

$$\psi^Z_{X/Y} = \frac{\omega_X - \omega_Z}{\omega_Y - \omega_Z} = \left.\frac{\omega_X}{\omega_Y}\right|_{\omega_Z=0} \qquad \eta^Z_{Y/X} = -\left.\frac{\bar{P}_Y}{\bar{P}_X}\right|_{\omega_Z=0} \tag{19}$$

Note that it is also $\psi^Z_{X/Y} = \phi^z_{x/y}(\tau_*)$, where τ_* is the overall speed ratio for which the PG is synchronous (see Eq. (12)).

Usually, these parameters are known with reference to the fixed-carrier condition and they are named respectively Willis' ratio $\Psi = \psi^C_{R/S}$ and basic efficiency $\eta_0 = \eta^C_{R/S}$. Nevertheless, in some cases it is needed to match a different permutation of *X*, *Y*, *Z*, depending on which p_x TPM power flow is known or more directly computable. In these cases,

$\psi^Z_{X/Y}$ can be calculated by the relationships of Table 1 as functions of Willis' ratio Ψ [38], while for $\eta^Z_{Y/X}$ we propose here a more straightforward formulation than [38]. Indeed, it is simply:

$$\eta^Z_{Y/X} = \psi^Z_{Y/X} / \bar{\psi}^Z_{Y/X} \tag{20}$$

where $\bar{\psi}^Z_{X/Y}$ is an adjusted fixed-*Z* speed ratio which can be yet obtained from Table 1 by replacing Ψ with Ψ/η_0.

$\boldsymbol{\psi^C_{R/S}}$	$\boldsymbol{\psi^C_{S/R}}$	$\boldsymbol{\psi^R_{S/C}}$	$\boldsymbol{\psi^R_{C/S}}$	$\boldsymbol{\psi^S_{C/R}}$	$\boldsymbol{\psi^S_{R/C}}$
Ψ	$\frac{1}{\Psi}$	$\frac{\Psi-1}{\Psi}$	$\frac{\Psi}{\Psi-1}$	$\frac{1}{1-\Psi}$	$1-\Psi$

Table 1. Relationships between the speed ratio of two PG shafts when the third one is motionless and the Willis' ratio.

For example, supposing that the fixed-*Z* apparent efficiency of our interest is $\eta^S_{R/C}$, we have:

$$\begin{cases} \bar{T}_C + \bar{T}_R + \bar{T}_S = 0 \\ \Psi = \dfrac{\omega_R - \omega_C}{\omega_S - \omega_C} \\ \eta_0 = -\dfrac{\bar{T}_R}{\bar{T}_S}\dfrac{\omega_R}{\omega_S}\Big|_{\omega_C=0} \end{cases} \Rightarrow \quad \frac{\bar{T}_R}{\bar{T}_C} = -\frac{1}{1-\Psi/\eta_0} \qquad \frac{\omega_R}{\omega_C}\Big|_{\omega_S=0} = 1-\Psi = \psi^S_{R/C} \tag{21}$$

hence:

$$\eta^S_{R/C} = -\frac{\bar{T}_R}{\bar{T}_C}\frac{\omega_R}{\omega_C}\Big|_{\omega_S=0} = \frac{1-\Psi}{1-\Psi/\eta_0} = \psi^S_{R/C}/\bar{\psi}^S_{R/C} \tag{22}$$

and similarly, for the other cases. Furthermore, it is useful to highlight that since Eq. (18) is valid only if $\eta^Z_{Y/X}$ is high, and this occurs for the common values of η_0 if it is $\Psi < 0.5$ or $\Psi > 2$ [38], then $\eta^Z_{Y/X}$ and its reciprocal $\eta^Z_{X/Y}$ can be used interchangeably in Eq. (18). In fact, [38] itself have proved that if $\eta^Z_{Y/X} \to 1$ then $1/\eta^Z_{Y/X} \cong 2 - \eta^Z_{Y/X}$ and therefore Eq. (18) remains unchanged. This implies that the definition of the only *Z* is sufficient to assess the fixed-*Z* apparent efficiency.

For a given input and output power, the PSU mechanical losses have to be compensated by the electric machines whose real powers can be directly obtained by reworking the formulas of [38] as follows:

$$\bar{p}_o = p_o - \frac{\tau_o}{\tau_{o_{\#i}}}\left[\bar{p}_L + \left(\frac{\partial \bar{p}_L}{\partial \tau} + \frac{\partial \bar{p}_L}{\partial \eta}\frac{\eta}{\tau}\right)(\tau_{\#i} - \tau)\right] \qquad \bar{p}_i = p_i - \frac{\tau_i}{\tau_{i_{\#o}}}\left[\bar{p}_L + \left(\frac{\partial \bar{p}_L}{\partial \tau} + \frac{\partial \bar{p}_L}{\partial \eta}\frac{\eta}{\tau}\right)(\tau_{\#o} - \tau)\right] \tag{23}$$

Once assessed the real CVU power flows, the real torque ratios $\bar{\theta}_o$ and $\bar{\theta}_i$ can be swiftly evaluated by dividing $\bar{p}_o$ and $\bar{p}_i$ to τ_o and τ_i, respectively.

3. FULL ELECTRIC VEHICLE

The parametric model described in the previous section is suitable for comprehensively analyzing any PS-CVT with two DOFs for both speeds (Eqs. (4)) and torques (Eqs. (7)) or powers (Eqs. (10)).

In this section, we rearrange the previous formulas of section 2 to assess the mechanical power losses occurring in the PSU and the resultant power flowing into the electric machines in Full Electric Vehicle operation (FEV), whereby the ICE is switched off and the vehicle is propelled by the electric motors. Nonetheless, whilst for a power-split functioning it is convenient referring the variables to the input shaft, the normalization to T_{in} and P_{in} is not advisable in FEV modes, as T_{in} is a reaction torque and P_{in} is null.

Indeed, in FEV functioning modes the shaft *in* (directly connected to the ICE) is kept motionless, thus only one kinematic DOF is available and the speed ratio between any two PSU branches is fixed and PGs are used only for torque multiplication from electric machines to the output. Therefore, the kinematic relationships (4) computed for $\omega_{in} = 0$ ($\tau \to \infty$) can be normalized to the output speed and are constant:

$$\frac{\omega_o}{\omega_{out}}\Big|_{\omega_{in}=0} = \frac{\tau_{o_{\#i}}}{\tau_{\#i} - \tau_{\#o}} \qquad \frac{\omega_i}{\omega_{out}}\Big|_{\omega_{in}=0} = \frac{\tau_{i_{\#o}}}{\tau_{\#o} - \tau_{\#i}} \qquad \frac{\omega_o}{\omega_i}\Big|_{\omega_{in}=0} = -\frac{\tau_{o_{\#i}}}{\tau_{i_{\#o}}} \tag{24}$$

The torques distribution can be derived from the ideal PSU power balance (5) computed for $P_{in} = 0$:

$$T_{out}\omega_{out} + T_o\omega_o + T_i\omega_i = 0 \tag{25}$$

By dividing Eq. (25) to ω_{out} and introducing Eqs. (24), the contribution of both electric motors to the output torque is:

$$T_{out} = \frac{\tau_{o_{\#i}}}{\tau_{\#o} - \tau_{\#i}}T_o + \frac{\tau_{i_{\#o}}}{\tau_{\#i} - \tau_{\#o}}T_i \tag{26}$$

In other words, given a certain P_{out} requested for vehicle propulsion, the power flowing in one electric motor can be freely selected, as opposed to the power-split operation where it would be more convenient to constrain the electric unit behavior to the input (ICE) and output powers (Eqs. (8)-(10)).

Furthermore, the same method proposed in section 2.3 enables the assessment of the PSU mechanical power losses occurring in FEV modes, if the power losses normalization is not performed to P_{in} as in Eqs. (17)-(18). However, $\eta_{X/x}$, $\eta^z_{Y/X}$ and $\psi^z_{X/Y}$ are not affected by the variation of the normalizing power and neither is the characteristic function $\phi^z_{x/y}$, being a powers ratio (Eq. (16)). Consequently, for FEV modes, $\phi^z_{x/y}$ can be easily computed by Eq. (11) for $\tau \to \infty$, by avoiding referring the branch *x* to a branch involving an infinite nodal ratio (such as the shaft *in*) to prevent numerical errors in $\phi^z_{x/y}$ computation. As a result, the mechanical power losses can be normalized to any PSU power flow, if also p_x is normalized to the same power. For convenience, we choose $-P_{out} = -\bar{P}_{out}$ as reference power (by considering the actual negative sign of P_{out}, because coming out from the PSU) and Eqs. (17)-(18) become:

$$\bar{p}'_L|_{OG} \approx -\left|\left(1-\eta_{X/x}\right) p'_x\right| \tag{27}$$

$$\bar{p}'_L|_{PG} \approx -\left|\left(1-\eta^z_{Y/X}\right)\left(\frac{\phi^z_{x/y}-\psi^z_{X/Y}}{1-\psi^z_{X/Y}}\right)p'_x\right| \tag{28}$$

where $\bar{p}'_L = -\bar{P}_L/P_{out}$ and $p'_x = -P_x/P_{out}$.

Moreover, the ideal power balance (25) becomes $p'_o + p'_i = 1$, from which $p'_o = 1 - p'_i$ and $p'_i = 1 - p'_o$. Instead, in real condition it is:

$$\bar{p}'_o + \bar{p}'_i + \bar{p}'_L = 1 \tag{29}$$

from which we can derive the real power flowing in one electric motor once fixed the real power flowing in the other motor and calculated the power losses. However, neither $\bar{p}'_o$ nor $\bar{p}'_i$ should take on negative values, thereby avoiding unnecessary CVU power recirculation. After assessing the real power ratios of the electric motors, the real torque ratios can be swiftly evaluated by dividing them by the speed ratios (24).

4. IDENTIFICATION OF THE FUNCTIONAL PARAMETERS

According to the previous section, any PS-CVT can be comprehensively described using a unique mathematical model based on nodal ratios and corresponding speed ratios. However, generally, manufacturers do not explicitly disclose these functional parameters, but they have to be derived from the constructive arrangement of the transmission. A first method that meets this objective was presented in [37]. It was based on the identification of four main groups, depending on the triad of main external shafts linked to each TPM. The equations for identifying the functional parameters were strictly dependent on the couple of the involved functional groups. Then, it required the standardization of the Willis' ratio depending on the position of the carrier, the sun gear and the ring gear. Furthermore, this identification procedure was suitable only for power-split transmissions with one or two TPMs.

The approach proposed in this section allows the calculation of the functional parameters from the constructive ones in a more straightforward way and regardless of the number of TPMs. Moreover, it does not require any case-related formulas, thus the computing process is easily automatable if performed in proper numerical software.

Before performing the calculation approach under consideration, we need to know:

- constructive parameters of the involved gear sets (i.e. PGs and OGs teeth ratios).
- mutual connections between the devices;

The aim is to evaluate the following parameters:

- nodal ratios, i.e. the mechanical points ($\tau_{\#o}$ and $\tau_{\#i}$) and the ones referred to the neutral nodes ($\tau_{\#n1}$, $\tau_{\#n2}$, …);
- corresponding speed ratios for each nodal ratio.

As it is explained in section 2.2, the number of proper nodal ratios equals the number of TPMs; each nodal ratio implies as many corresponding speed ratios as the number of TPMs minus one.

The functional parameters are obtained by performing matrix operations derived from the linear system of the kinematic constraints of the PSU:

$$[\mathbf{K}]\{\boldsymbol{\omega}\} = \{0\} \tag{30}$$

where $[\mathbf{K}]$ is the constraints matrix and $\{\boldsymbol{\omega}\}$ is a vector containing the rotational speeds of the PSU. As it will be evident later, to streamline the computational process, it would be better to sort the element in $\{\boldsymbol{\omega}\}$ so that the elements of the first rows are the rotational speeds of the main shafts, starting from ω_{out} and ω_{in} and then ω_o and ω_i, immediately followed by the ones referred to the neutral nodes and then all the others, and thus $\{\boldsymbol{\omega}\}$ is defined as follows:

$$\{\boldsymbol{\omega}\} = [\omega_{out} \quad \omega_{in} \quad \omega_o \quad \omega_i \quad \omega_{n1} \quad \omega_{n2} \quad \cdots]' \tag{31}$$

Each row of the matrix $[\mathbf{K}]$ reflects the kinematic constraints due to each mechanical device, hence $[\mathbf{K}]$ is a sparse matrix. In particular, for the *j*-th PG we can write:

$$\omega_{Cj}\left(1-\Psi_j\right) + \omega_{Sj}\left(\Psi_j\right) + \omega_{Rj}(-1) = 0 \tag{32}$$

where Ψ_j is the related Willis' ratio. For the *x*-th OG it is:

$$\omega_x(-1) + \omega_X(k_x) = 0 \tag{33}$$

An isokinetic joint linking two shafts is a particular OG with $k = 1$. Furthermore, a clutch can be mathematically modeled by fixed-ratio gears having a constructive ratio tending to ∞ when the clutch links a shaft to the framework, otherwise it acts as an isokinetic joint between the two involved shafts. Thus, Eq. (33) is sufficient to consider the variation of the internal connections in the PSU due to a mode shift, making this method well-suited even for multimode transmissions, usually complicated to analyze. It is worth noting that although assembling $[\mathbf{K}]$ is relatively trivial for a known PSU, designing a new one starting from scratch and generating a reasonable constraints matrix is a rather tricky

task, which has been the subject of extensive literature. In this respect, the graph theory [29]-[35] is widely used to explore the possible solutions; yet, identifying the most suitable layouts among the feasible ones is not immediate because there is no way to detect the best solution without simulating them all, and this requires using complex optimization algorithms and time-consuming calculations. On the contrary, the approach by functional parameters [36] makes the preliminary design of a new PS-CVT quite simple and fast.

The $[\mathbf{K}]$ matrix has as many rows as the constraints (N_C) are, i.e. the number of TPMs plus the further constraints realized by fixed-ratio gears, isokinetic joints, or clutches. The number of columns of $[\mathbf{K}]$ equals the number of rows of the $\{\boldsymbol{\omega}\}$ vector, which is $N_C + 2$ since the PSU has two degrees of freedom. Therefore, Eq. (30) is a linear system in N_C equations and $N_C + 2$ variables. By supposing that two of the variables (e.g. ω_{out} and ω_{in}) are known, we can write the rotational speed of the remaining PSU shafts as their function. For this purpose, it is necessary to perform a partition of the $[\mathbf{K}]$ matrix in order to obtain a two-column matrix $[\mathbf{W}]$, linking the rotational speeds of the PSU output and input to the other speeds contained in $\{\boldsymbol{\omega}\}$:

$$[\mathbf{K}]\{\boldsymbol{\omega}\} = \underbrace{\begin{bmatrix} k_{1,1} & k_{1,2} & k_{1,3} & \cdots & k_{1,N_C+2} \\ k_{2,1} & k_{2,2} & k_{2,3} & \cdots & k_{1,N_C+2} \\ k_{2,1} & k_{2,2} & k_{2,3} & \cdots & k_{1,N_C+2} \\ \vdots & \vdots & \vdots & \ddots & \vdots \\ k_{N_C,1} & k_{N_C,2} & k_{N_C,3} & \cdots & k_{N_C,N_C+2} \end{bmatrix}}_{[\mathbf{K}_{(1,2)}]\quad [\mathbf{K}_{1,2}]} \begin{matrix} \left.\begin{matrix} \omega_{out} \\ \omega_{in} \end{matrix}\right\} \{\boldsymbol{\omega}_{known}\} \\ \hline \left.\begin{matrix} \omega_o \\ \omega_i \\ \vdots \\ \omega_{N_C+2} \end{matrix}\right\} \{\boldsymbol{\omega}_{unknown}\} \end{matrix} = \{0\} \tag{34}$$

$[\mathbf{K}_{(1,2)}]$ is a submatrix of $[\mathbf{K}]$ that includes only its first two columns, while $[\mathbf{K}_{1,2}]$ is a submatrix of $[\mathbf{K}]$ obtained by removing them. Hence, the previous equation can be rewritten as follows:

$$[\mathbf{K}]\{\boldsymbol{\omega}\} = [\mathbf{K}_{(1,2)}]\{\boldsymbol{\omega}_{known}\} + [\mathbf{K}_{1,2}]\{\boldsymbol{\omega}_{unknown}\} = \{0\} \tag{35}$$

from which we can calculate the column vector of the unknown rotational speeds:

$$\{\boldsymbol{\omega}_{unknown}\} = -[\mathbf{K}_{1,2}]^{-1} \cdot [\mathbf{K}_{(1,2)}]\{\boldsymbol{\omega}_{known}\} \tag{36}$$

In other terms:

$$\begin{pmatrix} \omega_o \\ \omega_i \\ \omega_{n1} \\ \vdots \end{pmatrix}_{N_C x 1} = [\mathbf{W}] \begin{pmatrix} \omega_{out} \\ \omega_{in} \end{pmatrix} \tag{37}$$

where

$$[\mathbf{W}] = -[\mathbf{K}_{1,2}]^{-1} \cdot [\mathbf{K}_{(1,2)}] \tag{38}$$

Note that in Eq. (37) the vector of the unknown rotational speeds contains N_C elements. By using the MATLAB notation that can appear more familiar, Eq. (38) can be considered as follows:

$$[\mathbf{W}] = -[\mathbf{K}(:, 3{:}\,\mathrm{end})]^{-1}\,[\mathbf{K}(:, 1{:}\,2)] \tag{39}$$

At this point, the calculation of the functional parameters from the matrix $[\mathbf{W}]$ is straightforward. After normalizing Eq. (37) to ω_{in} we get:

$$\begin{pmatrix} \tau_o \\ \tau_i \\ \tau_{n1} \\ \vdots \end{pmatrix}_{N_C x 1} = \begin{bmatrix} w_{1,1} & w_{1,2} \\ w_{2,1} & w_{2,2} \\ \vdots & \vdots \\ w_{N_C,1} & w_{N_C,2} \end{bmatrix} \begin{pmatrix} \tau \\ 1 \end{pmatrix} \tag{40}$$

The first row of the system is:

$$\tau_o = w_{1,1}\tau + w_{1,2} \tag{41}$$

The previous equation computed for $\tau_o = 0$ leads to the calculation of the nodal ratio $\tau_{\#o}$:

$$0 = w_{1,1}\tau_{\#o} + w_{1,2} \qquad \Rightarrow \qquad \tau_{\#o} = -\frac{w_{1,2}}{w_{1,1}} \tag{42}$$

Obviously, $[\mathbf{W}]$ is speed-independent, since its terms are derived from the constructive constraints of Eqs. (32)-(33). Similarly, by calculating the second row for $\tau_i = 0$, we can obtain the nodal ratio $\tau_{\#i}$ as $-w_{2,2}/w_{2,1}$ and so on for the other nodal ratios. Thus, the nodal ratios are the opposite of the ratio between each element of the second column of $[\mathbf{W}]$ and the corresponding element in the first column. This operation is handily viable in MATLAB by using the element-wise division to obtain the nodal ratios vector:

$$\begin{pmatrix} \tau_{\#o} \\ \tau_{\#i} \\ \tau_{\#n1} \\ \vdots \end{pmatrix}_{N_C x 1} = -[\mathbf{W}(:,2)]\,./[\mathbf{W}(:,1)] \tag{43}$$

If the vector $\{\boldsymbol{\omega}\}$ is sorted properly (Eq. (31)), we can replace $[\mathbf{W}]$ with its submatrix $[\mathbf{W}^{(1,\dots,N_{TPM})}]$, which consists of the first N_{TPM}-th rows of $[\mathbf{W}]$, if N_{TPM} is the number of involved TPMs and thus of proper nodal ratios. In this way, we avoid the calculation of the nodal ratios related to the shafts rotating at one speed proportional to the speed of the main shafts and thus Eq. (43) returns a nodal ratios vector containing non-redundant elements.

The same simplified $[\mathbf{W}]$ matrix allows also the identification of the corresponding speed ratios. Indeed, when for example Eq. (40) is computed for $\tau = \tau_{\#o}$, it gives the corresponding speed ratios of the mechanical point of the electric machine O. The same is for the other nodal ratios. By properly assembling all the corresponding speed ratios we get a N_{TPM} by N_{TPM} square matrix whose diagonal elements are all equal to zero, while the other elements are the corresponding speed ratios:

$$\begin{bmatrix} 0 & \tau_{o_{\#i}} & \tau_{o_{\#n1}} & \cdots \\ \tau_{i_{\#o}} & 0 & \tau_{i_{\#n1}} & \cdots \\ \tau_{n1_{\#o}} & \tau_{n1_{\#i}} & 0 & \cdots \\ \vdots & \vdots & \vdots & \ddots \end{bmatrix}_{N_{TPM} x N_{TPM}} = \left[\mathbf{W}^{(1,\dots,N_{TPM})}\right] \begin{bmatrix} \tau_{\#o} & \tau_{\#i} & \tau_{\#n1} & \cdots \\ 1 & 1 & 1 & \cdots \end{bmatrix}_{2 x N_{TPM}} \tag{44}$$

5. EXAMPLE OF APPLICATION

This section aims to test the functionality of the novel procedure addressed in section 4 for identifying the functional parameters of any PS-CVT. To prove the flexibility of the model, we propose an exhaustive analysis of a complex multimode PS-CVT, the General Motors transmission of the Cadillac CT6 Luxury Sedan with a plug-in hybrid powertrain, whose constructive layout is showed schematically in Fig. 4. It is derived from the paper [39] submitted by the manufacturer and the patent [40]. In [15] Lee et al. used the lever analogy for investigating the mode selection of the Cadillac CT6 PS-CVT. They analyzed the efficiency of the transmission throughout the entire speed ratio range by supposing different loss factors in the electric power conversion occurring in the electric machines. The mechanical power

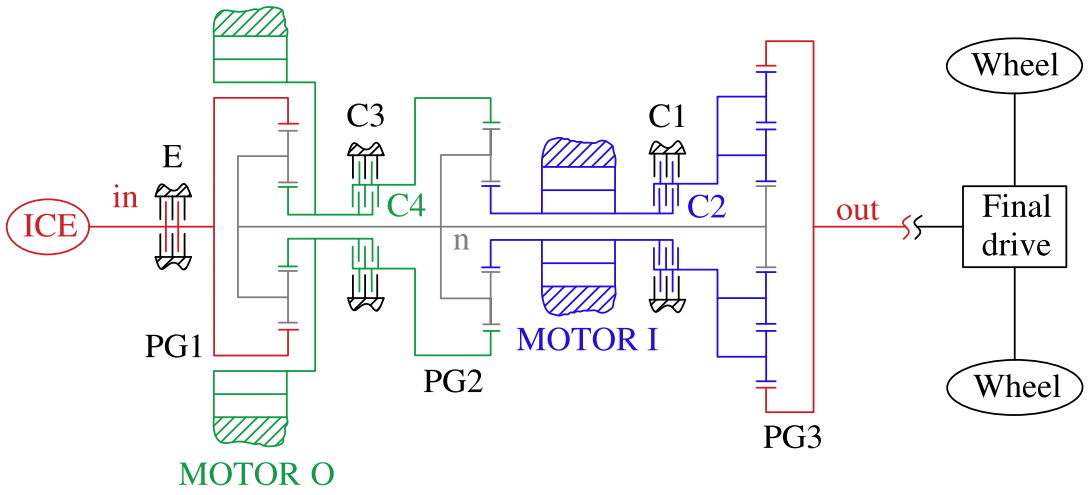

Fig. 4. Constructive layout of the Cadillac CT6 Plug-in HEV power-split CVT (derived from [40]).

losses were neglected. On the contrary, our application aims to deduce the range of utilization of each power-split mode starting from the basic functional parameters. These lead also to the calculation of the PSU mechanical power losses, which enable the calculation of the real power flowing in the electric unit (section 2.3).

The transmission under consideration consists of three planetary gear trains: PG1 and PG2 are identical and their Willis' ratio is $\Psi_1 = \Psi_2 = -0.505$; PG3 includes two sets of planet gears and its Willis' ratio is $\Psi_3 = 0.44$. The ICE is connected to the PG1 ring gear. The PG3 ring gear is the transmission output, which is connected to a final drive for delivering power to the wheels. In the following, the final drive is ignored because it does not affect the PSU behavior. Also, the PG1 carrier, the PG2 carrier and the PG3 sun gear are constrained to rotate together by a common shaft that is a neutral node. Furthermore, the powertrain involves two electric machines, equal in size, which can act as motors or as generators: Motor O is directly linked with the PG1 sun gear, Motor I is directly linked with the PG2 sun gear. Lastly, five multi-plate clutches potentially enable several different modes of operation. The half-stationary clutches C1 and C3 can act as a brake on the PG3 carrier and the PG2 ring gear, respectively. The fully-rotating clutch C2 can connect the PG2 sun gear (and thus Motor I) to the PG3 carrier, while the fully-rotating clutch C4 can connect the PG1 sun gear (and thus Motor O) to the PG2 ring gear. The clutch E prevents the ICE from moving and provides the reaction torque on the input shaft during full-electric functioning.

Clutches could be engaged in $2^5 = 32$ different arrangements, of which 16 are potential FEV modes (clutch E engaged) and the remaining 16 potential power-split hybrid operations [15]. However, not all alternatives are suitable for vehicle propulsion with available power on the output shaft. Indeed, the transmission with all the clutches opened has four available kinematic DOFs, i.e. two for each PG (six in total) minus two DOFs owing to the common shaft. Since each engaged clutch subtracts a further DOF, two clutches (not more and not less than two) among C1, C2, C3 and C4 must engage to achieve the power-split hybrid propulsion. However, C1 and C2, or C3 and C4 cannot be engaged at the same time otherwise the transmission is unable to transmit power to the output.

As a result, the viable power-split modes are only the four reported in Table 2. In particular, if clutches C1 and C3 are engaged, a Shunt input-split mode is achieved, since PG2 and PG3 are kinematically equivalent to an ordinary gear set and the output speed is proportional to the speed of Motor I. Another input-split mode is realized when C2 and C3 are both engaged because all the three PG3 branches rotate at proportional speed to the one of Motor I. By engaging the clutches C1 and C4, PG1 and PG2 operate in a Compound split mode, while PG3 acts as an OG. Finally, all the three PGs are active in a second Compound split mode, where C2 and C4 are engaged.

Mode	C1	C2	C3	C4	E
SHUNT 1	X		X		
PARALLEL 1	X		X	X	
COMPOUND 1	X			X	
PARALLEL 2	X	X		X	
COMPOUND 2		X		X	
PARALLEL 3		X	X	X	
SHUNT 2		X	X		
FEV 1	X		X		X
FEV 2	X			X	X
FEV 3			X	X	X
FEV 4		X	X		X

Table 2. Cadillac CT6 PS-CVT clutches operations for each of the eleven modes. Engaged clutches are marked with X.

If three clutches are engaged, the transmission has only one DOF and the overall speed ratio is fixed. This situation is useful when a motor is still at its mechanical point. Indeed, by closing a third clutch the reaction torque on the shaft that connects the motor to the PSU can be provided by the frame, rather than by the motor itself, which therefore is unloaded. This condition determines a fixed-ratio parallel hybrid mode, whereby a motor is switched off while the other electric machine can provide additional power for boosting the vehicle propulsion or can recharge the battery, but at a fixed speed ratio. However, since operating in a fixed-ratio parallel hybrid mode means operating in correspondence of a mechanical point of a power-split mode, it does not need to be addressed separately. Table 2 also shows that for each power-split mode there is a corresponding FEV mode, achieved by engaging the clutch E.

Fig. 5 summarizes the functional layout of the Cadillac CT6 transmission. With reference to the notation adopted in the previous sections, the subscripts *in*, *out*, *o* and *i* are referred to the PSU ports linked with the engine, PSU output, Motor O and Motor I, respectively. The neutral node is indicated by *n*.

Once identified the functional parameters for each power-split mode in section 5.1, these are used in section 5.2 to deduce the range of utilization of each mode by analyzing the rotational speed of the electric machines. Section 5.3 calculates the mechanical power losses and real CVU powers. The FEV operation is examined in section 5.4.

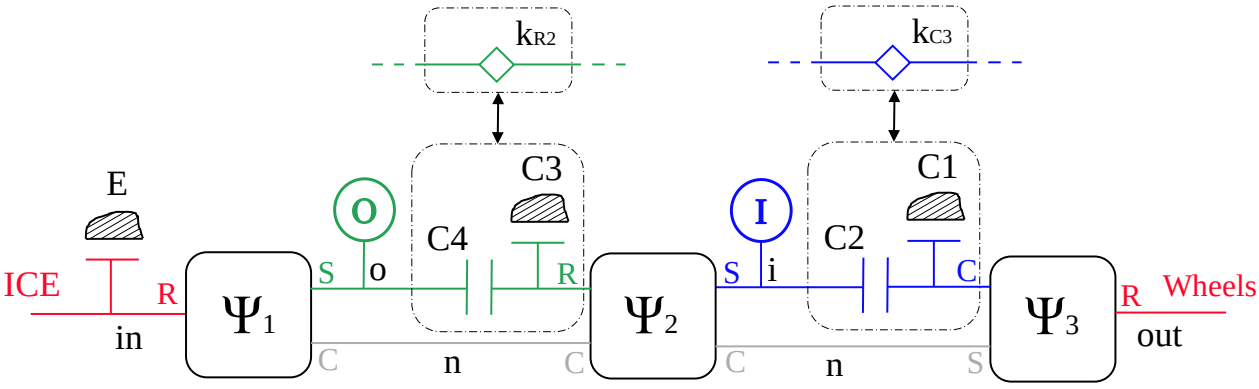

Fig. 5. Functional layout for Cadillac CT6 transmission and its operating modes.

5.1 Calculation of the functional parameters

In this section, the functional parameters are derived by applying the new method explained in section 4.

The first step is to determine the constraints matrix from the constructive arrangement of the PSU. As it is addressed in section 4, the constraints matrix [**K**] has as many rows as the number of constraints. Ignoring the simple isokinetic joints, which would cause redundant equations, the constructive constraints are related to the three PGs and the clutches system. In particular, the action of the clutch E is not taken into account throughout this evaluation because it only affects the full electric modes. Also, since the activation of C3 and C4 is mutually exclusive, they impose a single constraint on the shaft linked to the PG2 ring gear, which can be indicated by a fictitious fixed-ratio gear k_{R2} (Fig. 5) that switches from 1 to ∞ depending on the engaged clutch. The clutches C1 and C2, likewise, constrain the PG3 carrier acting like a fictitious fixed-ratio gear k_{C3}. Hence, there are 3+2 constraints: the [**K**] matrix dimension is 5x7 (i.e. N_C x ($N_C + 2$)), while the rotational speed vector $\{\boldsymbol{\omega}\}$ contains 7 elements ($N_C + 2$).

The rotational speed vector chosen to properly assemble [**K**] is:

$$\{\boldsymbol{\omega}\} = [\omega_{out} \quad \omega_{in} \quad \omega_o \quad \omega_i \quad \omega_n \quad \omega_{R2} \quad \omega_{C3}]'$$

The general constraint matrix related to the power-split modes is:

$$[\mathbf{K}] = \begin{bmatrix} 0 & -1 & \Psi_1 & 0 & 1-\Psi_1 & 0 & 0 \\ 0 & 0 & 0 & \Psi_2 & 1-\Psi_2 & -1 & 0 \\ -1 & 0 & 0 & 0 & \Psi_3 & 0 & 1-\Psi_3 \\ 0 & 0 & -1 & 0 & 0 & k_{R2} & 0 \\ 0 & 0 & 0 & -1 & 0 & 0 & k_{C3} \end{bmatrix}$$

where $k_{R2} = \omega_o/\omega_{R2}$ and $k_{C3} = \omega_i/\omega_{C3}$. According to Table 2 and Fig. 5, k_{R2} is equal to 1 when the clutch C4 is engaged (in Compound 1 and Compound 2 operating modes) or to ∞ when the clutch C3 is engaged (in Shunt 1 and Shunt 2). Similarly, k_{C3} is equal to 1 when the clutch C2 is active (in Compound 2 and Shunt 2) or to ∞ when the clutch C1 is active (in Shunt 1 and Compound 1).

After determining [**K**], we implemented the model in MATLAB and calculated the matrix [**W**] using Eq. (38). Exploiting some for-loops speeds up the replication of the same calculations for every mode. This makes the model highly automatable. In the numerical computing environment, we replaced ∞ with a value high enough (e.g., 10^5). Since there are three TPMs, only the first, second and third row of [**W**] are necessary to evaluate the nodal ratios and the corresponding speed ratios of the shafts *o*, *i* and *n* by Eqs. (43)-(44). The results are reported in Table 3.

Mode	$\tau_{\#o}$	$\tau_{\#i}$	$\tau_{\#n}$	$\tau_{o_{\#i}}$	$\tau_{o_{\#n}}$	$\tau_{i_{\#o}}$	$\tau_{i_{\#n}}$	$\tau_{n_{\#o}}$	$\tau_{n_{\#i}}$
SHUNT 1	0.29	0	0	-2.0	-2.0	2.0	0	0.66	0
COMPOUND 1	0.29	0.59	0	2.0	-2.0	2.0	3.9	0.66	1.3
COMPOUND 2	1.4	0.59	2.2	2.0	-2.0	2.0	3.9	0.66	1.3
SHUNT 2	1.4	0	0	-2.0	-2.0	2.0	0	0.66	0

Table 3. Nodal ratios and corresponding speed ratios for *o*, *i* and *n* for each power-split mode.

5.2 Kinematic analysis and mode shift

The mechanical points and the corresponding speed ratios characterize the CVU kinematic. The rotational speed of Motor O (τ_o) and Motor I (τ_i) are reported in Fig. 6 as a function of the overall transmission speed ratio τ.

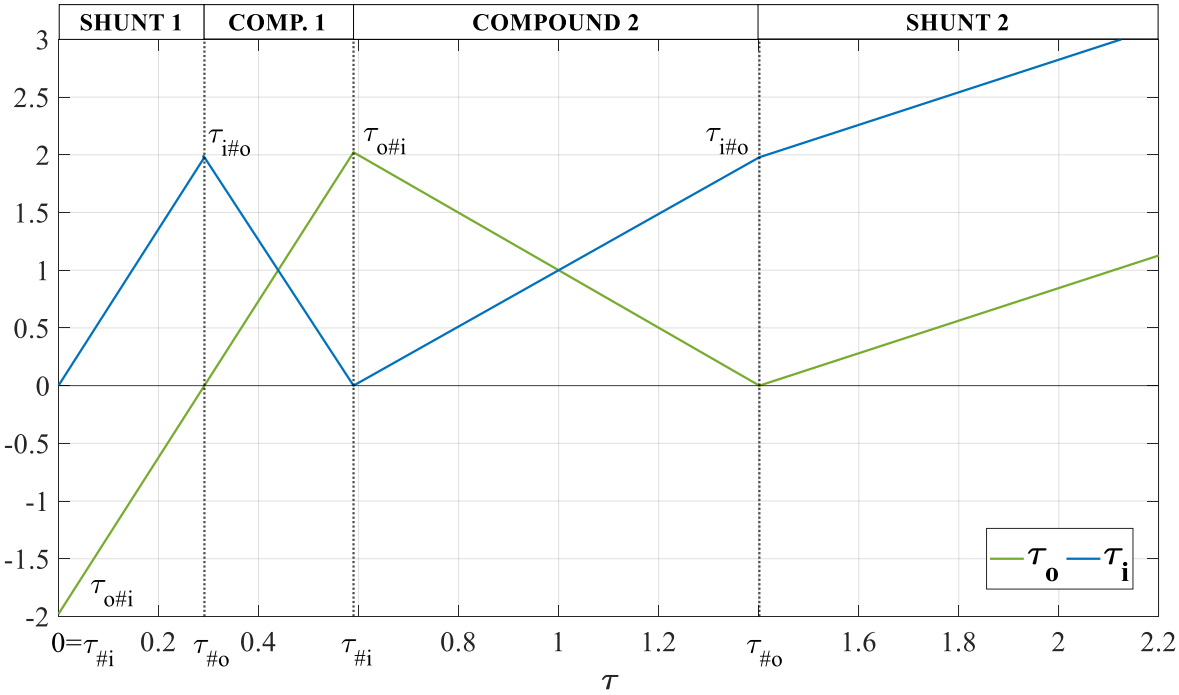

Fig. 6. Rotational speeds of Motor O (τ_o) and Motor I (τ_i).

It is noteworthy that each power-split mode could be ideally exploited for any overall transmission ratio τ, except that constructive constraints limit the maximum speed achievable by the electric machines. For this reason, there is the need to arrange multimode transmissions, which modify the PSU internal connections and thus the functional parameters, as well (Table 3). Different functional parameters involve different speed ratios (Fig. 6). However, it is advisable to perform the shift between two sequential modes to prevent clutches slipping. It is possible to realize a synchronous switch if the relative speeds of the involved shafts are null, i.e. in correspondence of the mechanical points, where one electric machine is motionless. Therefore, from Table 3 it is clear that the shift between Shunt 1 and Compound 1 must be performed in the common mechanical point $\tau_{\#o} = 0.29$, the shift between Compound 1 and Compound 2 must be performed in $\tau_{\#i} = 0.59$ and the shift between Compound 2 and Shunt 2 must be performed in $\tau_{\#o} = 1.4$ (Fig. 6).

Moreover, as stated before, the mechanical points can be exploited as fixed-ratio parallel hybrid modes. Thus, at $\tau_{\#i} = 0.59$ both the clutches C1 and C2, as well as C4, must engage to unload the Motor I. Instead, at $\tau_{\#o} = 0.29$ and $\tau_{\#o} = 1.4$ both the clutches C3 and C4, as well as C1 or C2 respectively, must engage to unload the Motor O.

To conclude the kinematic analysis of the transmission, we calculated the overall speed ratio for which every PG reaches its synchronism in each power-split mode (Eq. (15)). Obviously, the PGs operating like OGs throughout a certain power-split mode, do not reach the synchronous condition within that mode. Eventually, all the active PGs reach the synchronism at the same τ_* in Compound split modes because of the lack of OGs on the shaft connecting them.

	SHUNT 1	COMPOUND 1	COMPOUND 2	SHUNT 2
PG1	0.44	0.44	1.0	2.1
PG2	-	0.44	1.0	-
PG3	-	-	1.0	-

Table 4. Overall transmission ratio τ_* corresponding to the synchronism of each PG.

5.3 Mechanical power losses

According to section 2.3, the overall mechanical power losses result from the sum of the mechanical losses occurring in each PG. Any losses in the clutches are neglected. Thus, the total power losses are:

$$\bar{p}_L = \bar{p}_L|_{PG1} + \bar{p}_L|_{PG2} + \bar{p}_L|_{PG3}$$

which are calculated by Eq. (18), after labeling each branch of the TPMs as reported in Table 5. In this respect, it is worth noting that any reference notation can be applied, since the PGs mechanical power losses computed by Eq. (18) prescind from it, depending only on the relative motion between PG shafts and torques.

	x	*X*	*y*	*Y*	*z*	*Z*
PG1	*in*	ring	*o*	sun	*n*	carrier
PG2	*n*	carrier	*i*	sun	*o*	ring
PG3	*out*	ring	*n*	sun	*i*	carrier

Table 5. Reference notation of the TPMs shafts for the calculation of power losses in power-split modes.

Therefore:

$$\bar{p}_L|_{PG1} = -\left|(1-\eta^C)\left(\frac{\phi^n_{in/o}-\psi^C_{R/S}}{1-\psi^C_{R/S}}\right)p_{in}\right|$$

$$\bar{p}_L|_{PG2} = -\left|(1-\eta^R)\left(\frac{\phi^o_{n/i}-\psi^R_{C/S}}{1-\psi^R_{C/S}}\right)p_n\right|$$

$$\bar{p}_L|_{PG3} = -\left|(1-\eta^C)\left(\frac{\phi^i_{out/n}-\psi^C_{R/S}}{1-\psi^C_{R/S}}\right)p_{out}\right|$$

We chose the most convenient branch *x* for each PG. Indeed, $p_{in} = \bar{p}_{in} = 1$ and $p_{out} = \bar{p}_{out} = -\eta$ by definition. Furthermore, the real power transmitted by PG1 ring gear equals p_{in} and the real power transmitted by PG3 ring gear equals p_{out}, owing to the lack of OGs on the involved shafts. On the other hand, the power transmitted by the PG2 carrier can be calculated only in ideal conditions, by the principle of power conservation in the neutral node *n* and Eq. (16):

$$p_n|_{PG2} = -\,p_n|_{PG1} - p_n|_{PG3} = p_{in}\cdot\phi^o_{in/n} + p_{out}\cdot\phi^i_{out/n}$$

Table 6 summarizes the fixed-*Z* apparent efficiencies η^Z and the fixed-*Z* speed ratios $\psi^Z_{X/Y}$ for each PG, based on the functional and constructive layout of the transmission. The basic efficiency is supposed to be slightly lower for PG3 because it has one more gear meshing between the two sets of planet gears.

	Ψ	η_0	$\psi^Z_{X/Y}$	$\eta^Z = \psi^Z_{X/Y}/\bar{\psi}^Z_{X/Y}$
PG1	-0.505	0.97	Ψ	η_0
PG2	-0.505	0.97	$\dfrac{\Psi}{\Psi-1}$	$\dfrac{\Psi/(\Psi-1)}{\Psi/\eta_0/(\Psi/\eta_0-1)}$
PG3	0.44	0.96	Ψ	η_0

Table 6. Fixed-*Z* apparent efficiencies and fixed-*Z* speed ratios as functions of the basic efficiency η_0 and the Willis' ratio Ψ.

The involved characteristic functions are obtained by Eq. (11) using the proper nodal ratios from Table 3, as well as $\tau_{\#in} = 10^5$ and $\tau_{\#out} = 0$. At this point, the calculation of the power losses is straightforward and leads to the power losses map of Fig. 7, handled as a function of the overall transmission ratio τ and the overall apparent efficiency η. They are intended as a fraction of the input power and the contour spacing is 0.005. In both the compound-split modes, the power losses are minimum for τ = 0.44 and τ = 1, which correspond to synchronous conditions (see section 5.2).

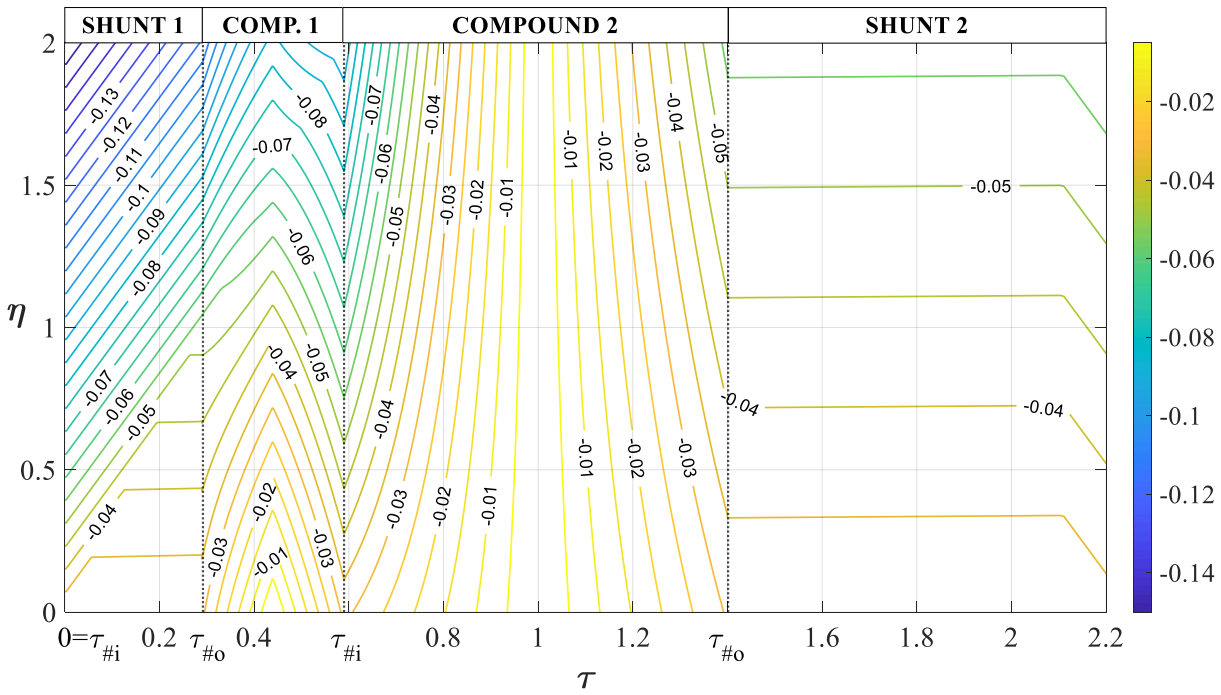

Fig. 7. Mechanical power losses occurring in power-split operation (as a fraction of the input power).

Once computed the power losses, the real power flowing in the electric machines are obtained by Eqs. (23) and shown in Fig. 8 (Motor O) and Fig. 9 (Motor I). The contour spacing is 0.1. Even though the power losses do not show any discontinuities, their gradient does, owing to a torque or speed reversal in the PSU. In other words, such discontinuities are due to an inversion of the basic efficiency η_0 occurred in PGs, but the addressed approximated method brings the advantage of not requiring to predict a priori any switch. The gradient discontinuity is reflected in real power flows near to the synchronism or the mode shift. The same trend would be noticed in real torques developed by the electric motors, which can be computed by dividing $\bar{p}_o$ by τ_o and $\bar{p}_i$ by τ_i.

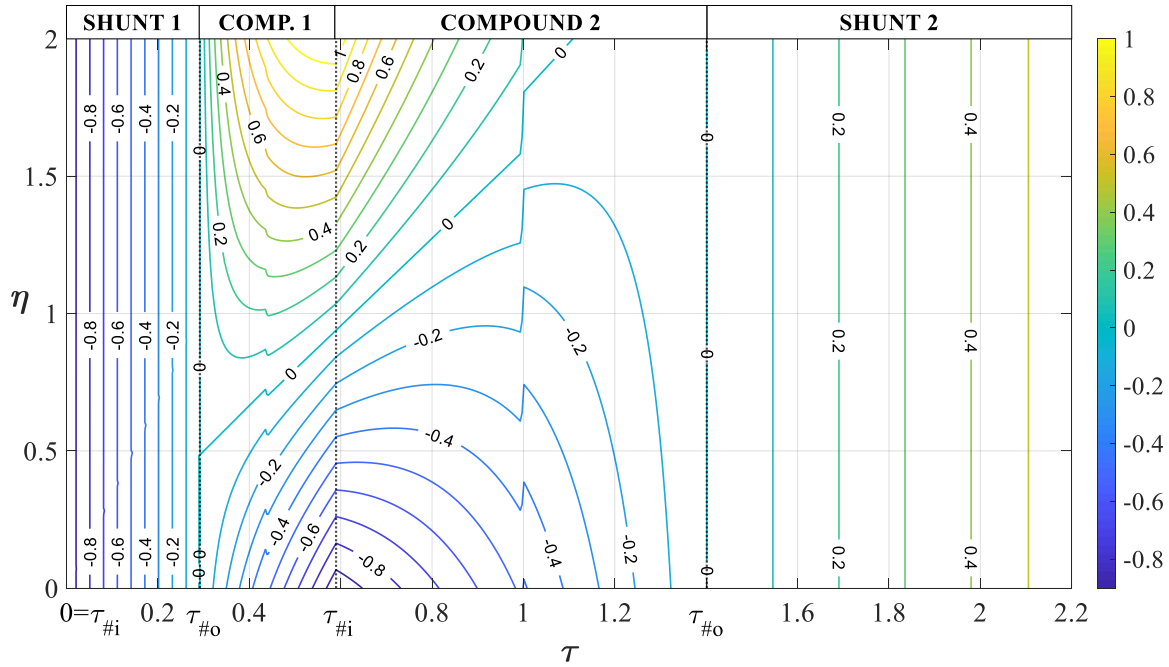

Fig. 8. Real power flowing through the Motor O (as a fraction of the input power).

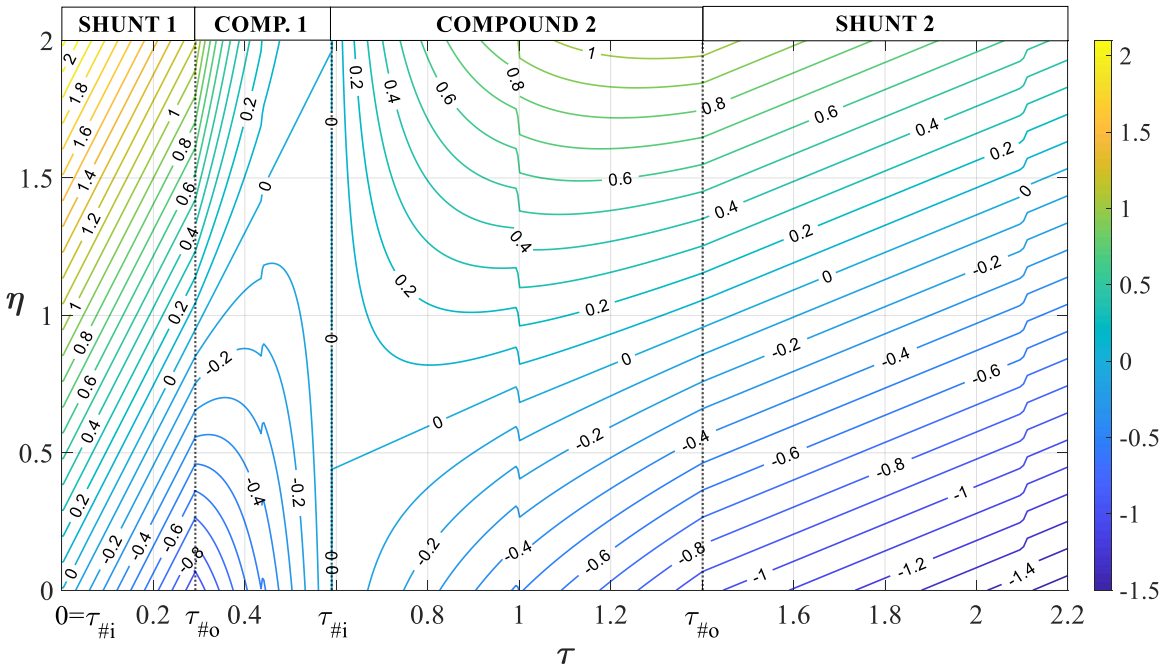

Fig. 9. Real power flowing through the Motor I (as a fraction of the input power).

5.4 Full electric operation

According to section 3, the same functional parameters of each power-split mode can be used to evaluate the transmission behavior in the respective FEV operation. Hence, this section analyzes the four FEV modes indicated in Table 2 and Fig. 5, by using the nodal ratios and the corresponding speed ratios of Table 3.

The ratios between the speed of electric machines and transmission output are computed by Eqs. (24) and shown in Table 7. They are constant, thus imposing ω_{out} implies univocal rotational speeds for both Motor O and Motor I. Furthermore, FEV 1 and FEV 2 achieve the highest speed ratios available among the FEV modes, which are very similar to the speed ratio between the Motor I and the output shaft realized for the fixed-ratio operation at the mechanical point $\tau = \tau_{\#o} = 0.29$. Therefore, both FEV 1 and FEV 2 might be used for providing acceleration at low vehicle speed, because of constructive constraints on the maximum speed achievable by the electric machines. The choice to exploit FEV 1 rather than FEV 2 or vice versa may be due to the mechanical power losses occurring in the PSU devices. On the other hand, the speed ratios of FEV 3 and FEV 4 are lower, therefore they can be used at higher vehicle speed. Nonetheless, the speed ratio of FEV 4 is the same speed ratio between the Motor I and the output shaft realized at the mechanical point $\tau = \tau_{\#o} = 1.4$ in hybrid operation. Since this fixed-ratio functioning point is exploited for overdrive, FEV 4 might not be suitable for pure electric propulsion because the vehicle usually achieves a lower maximum speed, and then the electric motors might be forced to operate at an inconveniently low speed. Moreover, Motor O and Motor I rotate at a very similar speed in all FEV modes (except for the direction of rotation in FEV 2 and FEV 3).

Mode	ω_o/ω_{out}	ω_i/ω_{out}	ω_o/ω_i
FEV 1	6.8	6.8	1.0
FEV 2	6.8	-6.6	-1.0
FEV 3	-2.5	2.4	-1.0
FEV 4	1.4	1.4	1.0

Table 7. Speed ratios in FEV modes.

The mechanical power losses in FEV modes are assessed by the same equations used in section 5.3 computed for $\tau = \tau_{\#in} = 10^5$ and normalized to the opposite of the output power. Moreover, we need to change the reference notation for PG1 to avoid the use of p_{in} (see section 3).

	x	***X***	***y***	***Y***	***z***	***Z***
PG1	*o*	sun	*in*	ring	*n*	carrier
PG2	*n*	carrier	*i*	sun	*o*	ring
PG3	*out*	ring	*n*	sun	*i*	carrier

Table 8. Reference notation of the TPMs shafts for the calculation of power losses in FEV modes.

The equations used for calculating power losses are:

$$\bar{p}'_L\big|_{PG1} = -\left|(1-\eta^C)\left(\frac{\phi^n_{o/in}-\psi^C_{S/R}}{1-\psi^C_{S/R}}\right)p'_o\right|$$

$$\bar{p}'_L\big|_{PG2} = -\left|(1-\eta^R)\left(\frac{\phi^o_{n/i}-\psi^R_{C/S}}{1-\psi^R_{C/S}}\right)p'_n\right|$$

$$\bar{p}'_L\big|_{PG3} = -\left|(1-\eta^C)\left(\frac{\phi^i_{out/n}-\psi^C_{R/S}}{1-\psi^C_{R/S}}\right)p'_{out}\right|$$

where $p'_{out} = \bar{p}'_{out} = -1$, while $p'_o\big|_{PG1}$ and $p'_n|_{PG2}$ must be assessed by combining Eq. (16) with the principle of power conservation:

$$p'_o\big|_{PG1} = p'_o - p'_o\big|_{PG2} = p'_o + \phi^n_{i/o}\cdot p'_i\big|_{PG2} = p'_o + \phi^n_{i/o}\cdot\left(p'_i - p'_i\big|_{PG3}\right) =$$
$$= p'_o + \phi^n_{i/o}\cdot\left(p'_i + \phi^n_{out/i}\cdot p'_{out}\right)$$
$$p'_n|_{PG2} = -p'_n|_{PG1} - p'_n|_{PG3} = p'_o\big|_{PG1}\cdot\phi^{in}_{o/n} + p'_{out}\cdot\phi^i_{out/n}$$

Fig. 10 shows the power losses as a function of $p'_i = -P_i/P_{out} = \bar{p}'_i$, Fig.11 shows the power flowing in Motor O and in Motor I in real condition, where $\bar{p}'_o = 1 - \bar{p}'_L - \bar{p}'_i$. Fig. 10 suggests that FEV 1 should be preferred to FEV 2 for lower vehicle speeds because of the lower power losses. Furthermore, the power losses occurring in FEV 1 are constant, therefore the PSU mechanical efficiency is not affected by the power rates provided by each motor. FEV 4 is the most efficient mode, thus, where possible, it should be preferred to FEV 3, which, on the contrary, is the least efficient. However, as stated before, FEV 4 might be unsuitable for pure electric propulsion, thus the exploitation of FEV 3 for the highest vehicle speeds may be unavoidable.

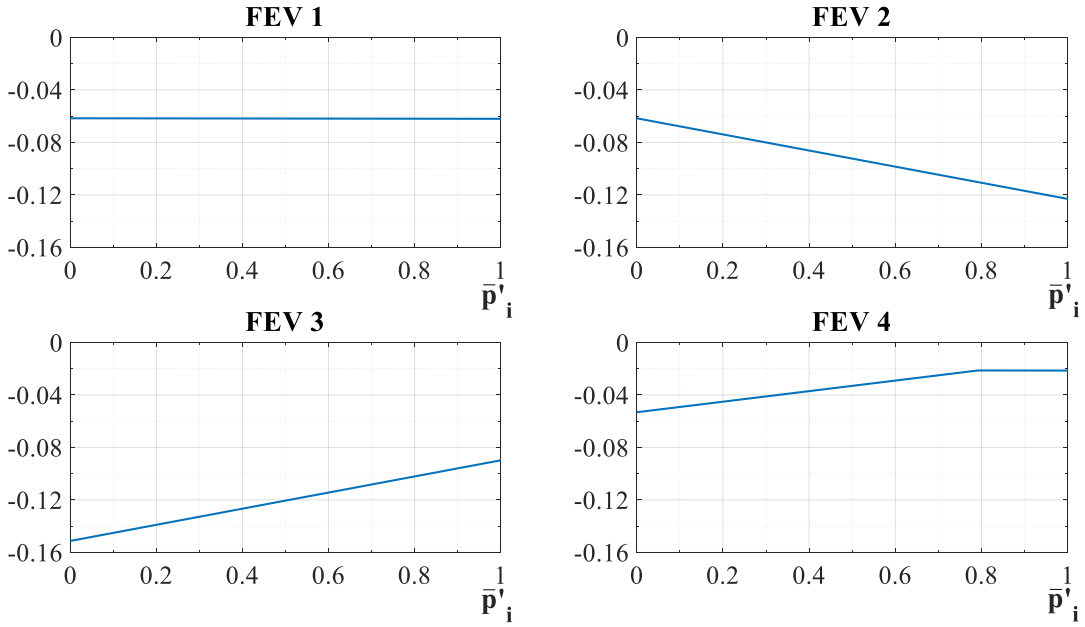

Fig. 10. Mechanical power losses occurring in FEV modes (as a fraction of the output power).

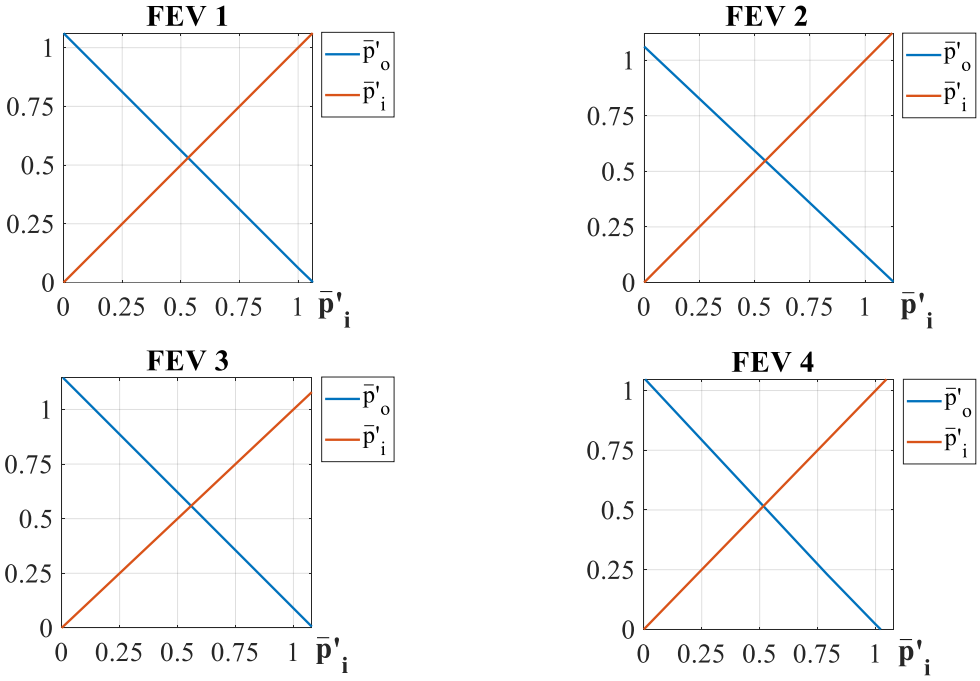

Fig. 11. Real power flowing in the electric motors in FEV modes (as a fraction of the output power).

6. CONCLUSIONS

The wide variety of the viable power-split transmissions requires to seek a proper mathematical model that can address PS-CVTs both in analysis and in the design phase. In this respect, the unified parametric model used in this paper emerges as a highly functional tool, particularly for modeling electric PS-CVTs. However, its use requires knowledge of the functional parameters on which it is based. The new method proposed in this study for the identification of these functional parameters starting from the transmission constructive layout was proven to be rapid and practical because it is easily automatable in numerical software. This new formulation is based on a matrix approach that befits any power-split transmission, regardless of the number of planetary gear sets and their constructive arrangement in the power-split unit, as well as of ordinary gearing or clutches. Indeed, it enables an effortless identification of the functional parameters even for multimode PS-CVTs.

Moreover, a rearrangement of the previous analysis model allowed us to assess the mechanical power losses occurring in the power-split unit and the consequent real power flowing into the electric machines, not only during hybrid-electric propulsion but also in pure electric operation.

Finally, the application of this model to the complex multimode PS-CVT of the Cadillac CT6 resulted in a comprehensive analysis of the kinematics, mechanical power losses and power flows when functioning in each of the eleven available functioning modes. However, the major strength of the model is to be highly versatile, and therefore it can be applied with equal ease to any other power-split transmission.

REFERENCES

[1] K. V. Singh, H. O. Bansal e D. Singh, A comprehensive review on hybrid electric vehicles: architectures and components, J. Mod. Transport. 27 (2019) 77–107.

[2] V. Krithika and C. Subramani, A comprehensive review on choice of hybrid vehicles and power converters, control strategies for hybrid electric vehicles, Int. J. Energy Resour. 42 (2018) 1789-1812.

[3] Y. Huang, N. C. Surawski, B. Organ, J. L. Zhou, O. H. H. Tang and E. F. Chan, Fuel consumption and emissions performance under real driving: Comparison between hybrid and conventional vehicles, Sci. Tot. Environ. 659 (2019) 275–282.

[4] C. Sieg and F. Küçükay, Benchmarking of Dedicated Hybrid Transmissions, Vehicles 2 (2020) 100–125.

[5] H. Chen, L. Li, A. Lange and F. Küçükay, Innovative Dedicated Hybrid Transmission Concepts in the Next Generation of Hybrid Powertrains, SAE Int. J. Alt. Power. 8(1) (2019) 75-88.

[6] Q. Li, X. Zhou, S. Wang and J. Liang, Power split transmission with continuously variable planetary ratio, Mech. Mach. Theory 140 (2019) 765-780.

[7] T. T. Ho and S. J. Hwang, Configuration Synthesis of Novel Hybrid Transmission Systems Using a Combination of a Ravigneaux Gear Train and a Simple Planetary Gear Train, Energies 13 (2020) 2333. DOI:10.3390/en13092333.

[8] W. Zhuang, S. Li, X. Zhang, D. Kum, Z. Song, G. Yin and F. Ju, A survey of powertrain configuration studies on hybrid electric vehicles, Appl. Energy 262 (2020) 114553. DOI: 10.1016/j.apenergy.2020.114553.

[9] P. Mattsson, Continuously Variable Split-Power Transmission with Several Modes, Chalmers University of Technology, Göteborg, Sweden, 1996.

[10] B. Conlon, Comparative analysis of single and combined hybrid electrically variable transmission operating modes, SAE World Congr. 2005 (2005).

[11] N. Kim, J. Kwon and A. Rousseau, Trade-off between Multi-mode Powertrain Complexity and Fuel Consumption, Proc. of the 25th World Battery, Hybrid and Fuel Cell Electr. Veh. Symp. & Exhib., Shenzhen, China, November 2010.

[12] H. Kim, T. Barhoumi and D. Kum, Comprehensive Design Methodology of Compound-Split Hybrid Electric Vehicles: Introduction of the Compound Lever as a Design Tool, IEEE Access 7 (2019) 84744–84756.

[13] W. Wang, R. Song, M. Guo and S. Liu, Analysis on compound-split configuration of power-split hybrid electric vehicle, Mech. Mach. Theory 78 (2014) 272-288.

[14] Y. G. Liao and M. Y. Chen, Analysis of multi-speed transmission and electrically continuous variable transmission using lever analogy method for speed ratio determination, Adv. Mech. Eng. 9 (8) (2017) 1–12.

[15] W. Lee, J. Park and N. Kim, Analysis of Transmission Efficiency of a Plug-In Hybrid Vehicle Based on Operating Modes, Int. J. Precis. Eng. Manuf. Green Technol. (2019). DOI: 10.1007/s40684-019-00147-9.

[16] X. Chen, J. Jiang, L. Zheng, H. Tang and X. Chen, Study and Analysis of a Multi-Mode Power Split Hybrid Transmission, World Electr. Veh. J. 11 (2020) 46. DOI:10.3390/wevj11020046.

[17] H. T. Ngo and H. S. Yan, Configuration synthesis of series-parallel hybrid transmissions, Proc. Inst. Mech. Eng. Part D (2015) 230.

[18] A. T. Zaremba, C. Soto and M. Jennings, Methodology for Assessment of Alternative Hybrid Electric Vehicle Powertrain System Architectures, SAE Int. J. Alt. Power. 1(1) (2012). DOI:10.4271/2012-01-1010.

[19] A. K. Gupta and C. P. Ramanarayanan, Analysis of circulating power within hybrid electric vehicle transmissions, Mech. Mach. Theory 64 (2013) 131-143.

[20] M. Cammalleri, Efficiency of Split-Way CVT's. A Simplified Model, SAE Technical Paper 2007-24-0133 (2007). DOI: 10.4271/2007-24-0133.

[21] E. Pennestrì, L, Mariti, P. P. Valentini and V. H. Mucino, Efficiency evaluation of gearboxes for parallel hybrid vehicles: Theory and applications, Mech. Mach. Theory 49 (2012) 157-176.

[22] P. Dong, Y. Liu, P. Tenbergec and X. Xu, Design and analysis of a novel multi-speed automatic transmission with four degrees-of-freedom, Mech. Mach. Theory 108 (2017) 83-96.

[23] D. Rotella, M. Cammalleri, D. Qin and X. Zhou, A Simple Method for the Design of Hybrid Electric Power-Split CVTs: A Case Study, IFToMM ITALY 2018, Mech. Mach. Sci. 68 (2019) 70–79. DOI: 10.1007/978-3-030-03320-0_8.

[24] A. Rossetti, A. Macor, Continuous formulation of the layout of a hydromechanical transmission, Mech. Mach. Theory 133 (2019) 545-558.

[25] F. Bottiglione, S. De Pinto and G. Mantriota, Infinitely Variable Transmissions in neutral gear: Torque ratio and power re-circulation, Mech. Mach. Theory 74 (2014) 285-298.

[26] S. De Pinto and G. Mantriota, Power Flows in Compound Transmissions for Hybrid Vehicles, Machines 7 (2019) 19. DOI: 10.3390/machines7010019.

[27] S. De Pinto and G. Mantriota, A simple model for compound split transmissions, Proc. Inst. Mech. Eng. Part D 228 (2014) 549-564.

[28] F. Bottiglione and G. Mantriota, Power Flows and Efficiency of Output Compound e-CVT, Int. J. Veh. Technol. 2015 (2015) 136437.

[29] H. Pei, X. Hu, Y. Yang, X. Tang, C. Hou and D. Cao, Configuration optimization for improving fuel efficiency of power split hybrid powertrains with a single planetary gear, Appl. Energy 214 (2018) 103-116.

[30] M. Du and L. Yang, A basis for the computer-aided design of the topological structure of planetary gear trains, Mech. Mach. Theory 145 (2020) 103690.

[31] V. R. Shanmukhasundaram, Y. V. D. Rao and S. P. Regalla, Enumeration of displacement graphs of epicyclic gear train from a given rotation graph using concept of building of kinematic units, Mech. Mach. Theory 134 (2019) 393-424.

[32] F. Yang, J. Feng and H. Zhang, Power flow and efficiency analysis of multi-flow planetary gear trains, Mech. Mach. Theory 92 (2015) 86-99.

[33] J. R. Gomà Ayats, U. Diego-Ayala, J. Minguella Canela, F. Fenollosa and J. Vivancos, Hypergraphs for the analysis of complex mechanisms comprising planetary gear trains and other variable or fixed transmissions, Mech. Mach. Theory 51 (2012) 217-229.

[34] D. R. Salgado and J. M. Del Castillo, Analysis of the transmission ratio and efficiency ranges of the four-, five-, and six-link planetary gear trains, Mech. Mach. Theory 73 (2014) 218-243.

[35] X. Zhou, D. Qin, D. Rotella and M. Cammalleri, Hybrid Electric Vehicle Powertrain Design: Construction of Topologies and Initial Design Schemes, IFToMM ITALY 2018, Mech. Mach. Sci. 68 (2019) 49–60. DOI: https://doi.org/10.1007/978-3-030-03320-0_6.

[36] M. Cammalleri and D. Rotella, Functional design of power-split CVTs: an uncoupled hierarchical optimized model, Mech. Mach. Theory 116 (2017) 294–309.

[37] D. Rotella and M. Cammalleri, Direct analysis of power-split CVTs: a unified method, Mech. Mach. Theory 121 (2018) 116–127.

[38] D. Rotella and M. Cammalleri, Power losses in power-split CVTs: a fast black-box approximate method, Mech. Mach. Theory 128 (2018) 528–543.

[39] A. Holmes, J. Liu, D. Ames, V. Neelakantan, K. Rahman and T. Grewe, General Motors Electric Variable Transmission for Cadillac CT6 Sedan, SAE Technical Paper 2016-01-1150 (2018). DOI: 10.4271/2016-01-1150.

[40] A. G. Holmes, M. R. Schmidt, D. Klemen and B. M. Conlon, Three mode electrically variable transmission, US Patent 7,645,206 B2, 2010.